Micro CT based stochastic design and flow analysis of dry fiber preforms manufactured by automated fiber placement

Muhammad A. Ali[1], Tayyab Khan[1], Kamran A Khan[1], Rehan Umer*[1]
[1]Department of Aerospace Engineering, Khalifa University of Science and Technology, Abu Dhabi, UAE.
*Corresponding Author Email: rehan.umer@ku.ac.ae

ABSTRACT

The effective design of channels in dry tape preforms is crucial for achieving desired preform permeability for successful resin injection for composites manufacturing using Automated Fiber Placement (AFP) process. Achieving target gaps and their locations in the AFP layup is extremely challenging. This work investigates the correlation between the spatial variability of the preforms and the in-plane permeability using an X-ray Computed Tomography (XCT) based characterization framework. The tomographic images of two different dry carbon tape preforms with different tape widths were used to generate realistic and XCT based stochastic models to be used for numerical permeability predictions. The variability in the tape placement by the robotic head and its effect on preform permeability was also examined through stochastic geometric modeling of the laid preform. A benchmark transient permeability measurement set-up was utilized to obtain experimental in-plane preform permeability through 2D radial mold filling. The in-plane numerical permeability values showed significant scatter, with a coefficient of variance of 75-130%, which deviated from the experimental measurements by approximately one order of magnitude. These findings strongly re-affirm that the experimental permeability measurement technique based on transient mold filling of dry fiber AFP preforms is complex however, the XCT based stochastic modeling technique is an effective way to estimate the permeability of dry fiber AFP preforms virtually.

Keywords: X-ray Computed Tomography; Automated fiber placement; Resin flow; Process Modeling.

1. Introduction

Reinforcement layup and preforming is one of the crucial steps in any composites manufacturing process including liquid composite molding (LCM) [1-5]. In LCM, the preforming step represent assembly of dry fabrics into a mold cavity before injection of liquid resin after mold closure. Traditionally, preforming step has been achieved by laying and draping 2D and 3D reinforcements. These fabrics are either woven, stitched, or bonded together and draped inside the mold to conform to the feature of the mold. The preforming step requires sophisticated textile processing capabilities which are not only lengthy and costly but also involve manual labor. The automated fiber placement (AFP) [6-8] is a technology that overcomes many of the preforming problems through the utilization of a robotic arm. The robotic arm carrying creels of fibers maneuvers through complex mold surfaces, and deposits fibers with desirable load-related fiber orientations and minimum fiber crimp and undulations [9]. The deposited fibers can be in the form of tapes, tow-pregs or dry fibers [9]. This technology has been successfully used on a number of modern aircraft structures such as fuselages, frames, wing box etc. [10-13]. It is well-established that the AFP technique is one of the most advanced composites manufacturing techniques, especially for manufacturing large-scale aero-structures [9].

Dry tape manufacturers have been using binding agents in the form of powders with AFP preforms to obtain good tacking properties. The use of a thin, highly permeable surface veil on the dry tows gives better resin impregnation characteristics and develops a biding agent for subsequent layers during placement process [10, 11]. The binding material is usually activated through a powerful heating element such as laser, which is generally installed in the AFP head. Additionally, the response time of the heating element is desired to be rapid enough to prevent any ply spring-back [14] due to viscoelastic compaction behavior, a phenomena frequently encountered in fiber

reinforcements for LCM processes [15, 16]. Along with this, the final part quality in the AFP process is significantly influenced by the compression of the tape through the compaction rollers, considering that the first layer is compressed multiple times while the last layer is only compressed once. As a result, the preform may be nonhomogeneous (in the through-thickness direction) leading to non-uniform flow channels in the in-plane direction.

The dry fibers or tapes provide significant advantages over pre-impregnated tapes in terms of cost [10, 11], shelf life and ease of material handling [7, 17, 18]. However, the poor resin impregnation behavior of dry tape preforms remains a major challenge compared with woven and non-crimp stitched fabrics. The dry tapes have relatively low permeability which is a dominant factor in LCM process [17, 19-21]. For example, the permeability of dry fiber AFP performs at fiber volume fraction of 50% in the through thickness direction is approximately 1×10^{-15} to 5×10^{-14} m^2 which is one or two orders lower than woven and non-crimp fabrics at the same fiber volume fraction [22]. Recently, several efforts have been made to understand the impact of various methods and procedures to enhance the overall permeability of the preforms manufactured by dry fiber AFP. Rimmel et al. [11] showed that stitching of the preform causes meso-scale channels and flow paths in the thickness direction and hence, increasing the out-of-plane permeability. In another study [23], it was demonstrated that the permeability in the plane of the preform can largely be affected by stitching the layers together. A similar approach was also applied for AFP preforms [22]. In our recent work [24], we analyzed the effect of different dry tape channel sizes and tape overlap rate on the through thickness permeability of the preform. It was found that the permeability was predominantly effected (60% contribution) by the channel size variations between the dry tapes. The channels in dry fiber AFP preforms can create meso-scale flow channels and enhance in-plane permeability. The optimized channels can play a vital role in better distribution of the resin, since

the flow velocity within these channel is many orders higher than the flow through micro-level flow channels (i.e., with in the fiber rovings) at same pressure differential [25]. Therefore, the channel size in dry fiber AFP preforms is one of the most critical parameters to address for achieving desired preform permeability for successful resin infusion.

In order to enhance the permeability of the AFP preform, several experimental studies were conducted and analyzed the effect of varying the channel sizes, binder amount, lay up sequence and tufting of preforms on permeability values [11, 26]. A systematic study to understand the impregnation behavior of AFP preforms, and the effects of different geometric parameters on its in-plane permeability does not currently exist. Therefore, there is a need to create new procedures and concepts that can offer the possibility to enhance in-plane and out-of-plane permeability values up to the level of conventional fabrics. Because of the variability of the fabric architecture, it is quite challenging to precisely predict preform permeability and require advanced modeling techniques to bring the permeability predictions much closer to experimental values [27, 28].

The primary objective of this research is to correlate the variability of channels created for dry tape preforms using the automated dry fiber placement process for in-plane permeability. A novel XCT based characterization framework was utilized to scan two different tape width preforms. These scans allowed capturing realistic and accurate geometric models for numerical permeability predictions. The scanned preforms were also re-constructed in TexGen software, and the numerically predicted in-plane permeability values were compared with the experimental measurements. A benchmark permeability measurement set-up was utilized to obtain experimental in-plane preform permeability through 2D radial transient mold filling. The effect of robotic tape placement variability on variations in permeability predictions was also examined in detail through stochastic geometric modeling of preform variability.

2. Experimental

2.1 Materials

The dry carbon fiber tapes supplied by Solvay, Wrexham, UK (Prism TX1100®) were used in this study. The tapes, with a thickness of 0.2 mm, comprised of unidirectional Tenax IMS65 carbon fibers having fiber diameter of approximately 5 µm. Two preforms were manufactured using these dry tapes through AFP manufacturing process quarter inch (6.35 mm) and a half inch (12.7 mm) wide tape. The tapes incorporate thermoplastic binder, and a proprietary surface veil, the binder is activated by the heating action of laser beam attached to the Coriolis AFP head. The dry tapes were bound by the melting of the thermoplastic binder and compression of the AFP roller. The tape gaps were adjusted prior to manufacturing, a target channel of 0.2 mm between the dry tapes was considered, as shown in Figure 1a. The preforms consist 24 layers of dry tape stacked in a quasi-isotropic sequence of $[+45/0/-45/90]_{3s}$ as shown in Figure 1b. The total thickness of both the preforms, including the binder and surface veil, was about 5.15 mm.

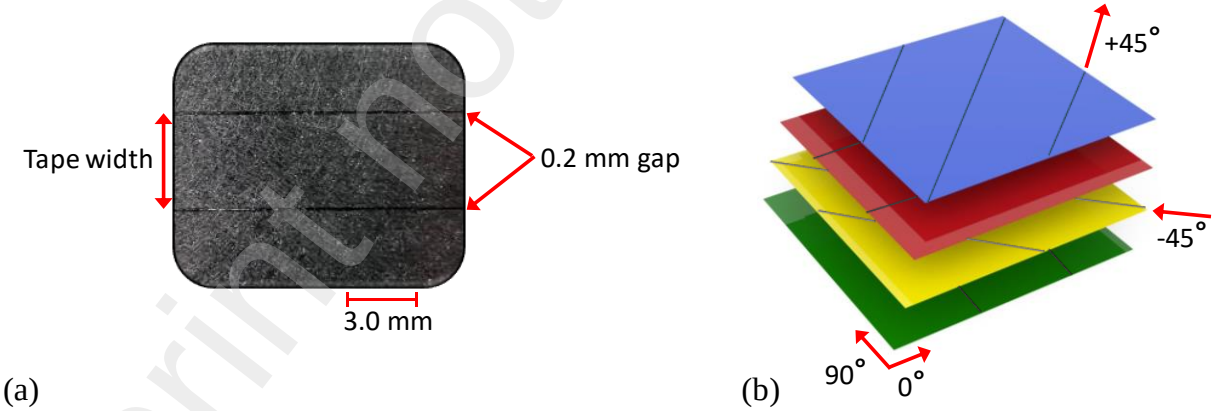

Figure 1. Material description (a) top view and (b) lay-up sequence.

2.2 In-plane Permeability Measurement Setup

The in-plane permeability values of the preforms were experimentally measured using the radial injection method. The radial injection fixture is housed on an MTS UTM frame as shown in Figure

2a. A circular plate (Ø250 mm), with an injection hole (Ø10 mm) in the middle, was attached to the crosshead of the MTS machine. The top plate was attached such that a parallel and uniform load is applied to the compacted preform before injection. For injecting the test fluid, the injection hole was connected to the fluid supply line via a hole drilled from the side of the top plate. The inlet pressure was measured through a pressure sensor connected at the end of the fluid supply line, as shown in Figure 2a. The test specimens were placed on a square glass plate (300×300 mm^2) supported by an aluminum structure fixed at the bottom of the MTS UTM frame. Compressed air was supplied to a pressure pot having pressure regulator to control the injection pressure. A video camera was placed under the glass plate to capture the flow of the fluid. It was ensured that the test environment had appropriate lighting to capture videos with clear contrast between the fluid and the background. The LabVIEW software was used to acquire important experimental parameters such as, injection pressure and test fluid temperature. The overall setup showing its components is illustrated schematically in Figure 2b. Test samples having a diameter of 200 mm were prepared using a clicker die cutting press. A 10 mm hole was created by using a punch in the test samples. While placing the preform sample on the glass plate, it was ensured that the punched hole aligned well with the injection hole. The test fluid was injected at a constant pressure of 1.5 bars (150 kPa) until the preform was fully saturated. Shell Tellus S2 M32 hydraulic oil was used as test fluid to measure the preform permeability having a viscosity of 0.086 Pa.s at room temperature.

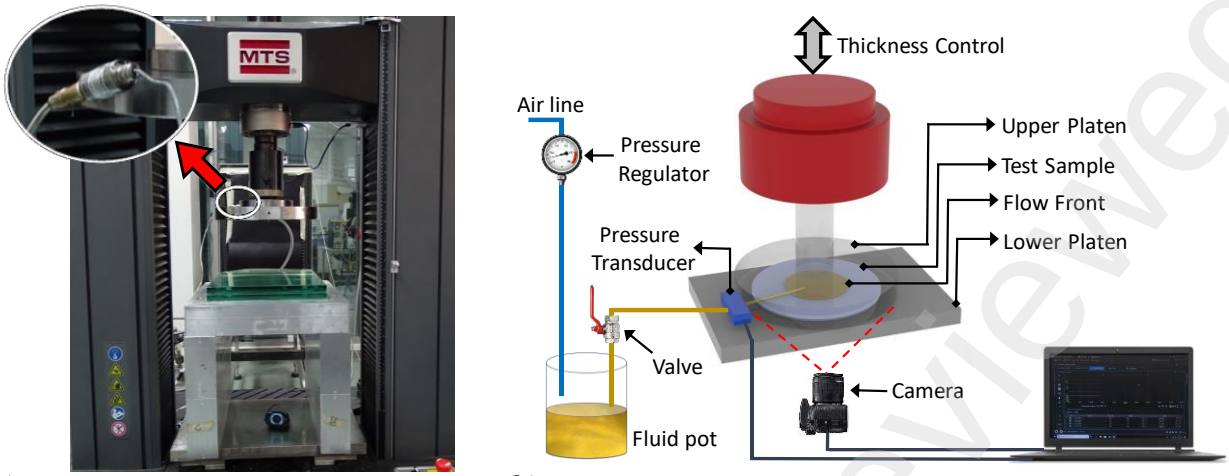

(a) (b)

Figure 2. Experimental setup for in-plane permeability measurements, (a) photograph of the test fixture showing the inlet pressure sensor, and (b) schematic illustration of the overall setup.

2.3 Image Processing

The recorded video was analyzed and the flow front progression with time was determined after several image processing steps using MATLAB®. The step-by-step procedure is shown in Figure 3. Frames of the video were captured after every 10 seconds and the raw images were cropped and aligned with the tapes oriented in +45° orientation. This orientation was chosen as it was the only identifiable direction in the video. A mask was applied on the images to hide the corners and isolate the flow region from the unnecessary background. The contrast of the images was enhanced for better flow front edge detection and then binary images were created. After image processing, dry and wet regions appeared as black and white respectively. The coordinates of the flow front were determined by tracing the boundary of the wet region and were converted from pixels to physical units using a conversion scale. The conversion scale was established by measuring the diameter of the test sample in terms of number of pixels and then comparing it to the actual diameter measured in millimeters. Finally, the flow front was fitted with an ellipse approximated by using least square fitting procedure using a Matlab code. Note that the principle axes of these ellipses were aligned with the tapes oriented in +45° and -45° orientations.

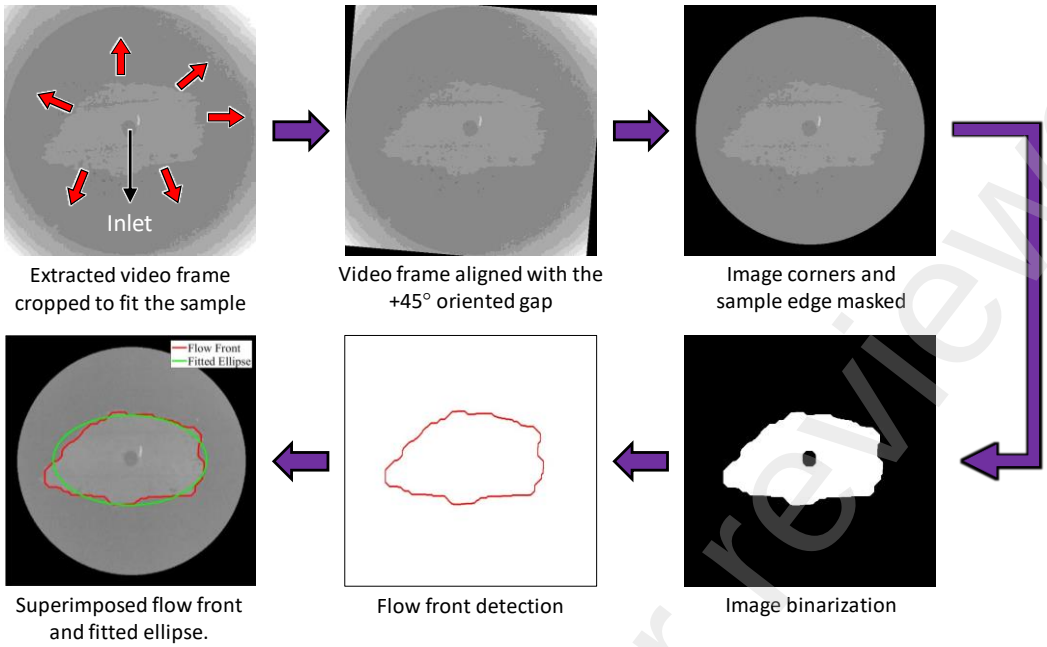

Figure 3. Step-by-step image processing procedure for the flow front detection using MATLAB.

2.4 Permeability Computation

The principal axes of the ellipses fitted to the flow front was measured as a function of time. Since, the principle axes of these ellipses were aligned with the tapes oriented in +45° and -45° orientations, the permeability values are symbolised as K_{+45} and K_{-45}, instead of K_{11} and K_{22}. Also, the major and minor axes of the ellipses were aligned with the +45° and -45° orientations, respectively. Using the measured principal axes of the fitted ellipses, the principal in-plane permeability values K_{+45} and K_{-45} were calculated using the method formulated by Weitzenböck et. al. [29-31]. In this method, the principle permeability values are given by the following equations,

$$K_{+45} = \frac{\mu\varphi}{4t\Delta P}\left\{x_f^2\left[2\ln\left(\frac{x_f}{x_o}-1\right)+x_o^2\right]\right\} \quad (1)$$

$$K_{-45} = \frac{\mu\varphi}{4t\Delta P}\left\{y_f^2\left[2\ln\left(\frac{y_f}{y_o}-1\right)+y_o^2\right]\right\} \quad (2)$$

where x_f and y_f are the major and minor axes of the ellipses and x_0 and y_0 are the radial dimensions of the inlet hole in the given directions (+45° and -45° orientations). The term ΔP is the pressure difference between the injection point and the flow front location at a given time t, and φ is defined as the porosity of the preform.

2.5 XCT Measurements and Analysis

To investigate the microstructure of the preform, especially in terms of the variability of channels between the adjacent tapes during layup, a non-destructive characterization framework was employed. The characterization framework consisted of a GE® Phoenix Nanotom device which was used to obtain micro-CT images of the test samples. The test samples were circular discs of 40 mm diameter and were scanned at a resolution of 25 µm. Further details about the micro-CT image acquisition setup and the scanning procedure can be found in our previous works [24, 32-34]. The micro-CT images were used to reconstruct grey scale raw volumes of the test specimens. The reconstructed raw volumes of the preforms with quarter and half inch tapes are shown in Figure 4. These grey scale raw volumes were directly converted into computational domains for virtual permeability computation through digital flow simulations. Additionally, stochastic models were also generated using the statistical distribution of the channel sizes measured from slices extracted from the raw volumes.

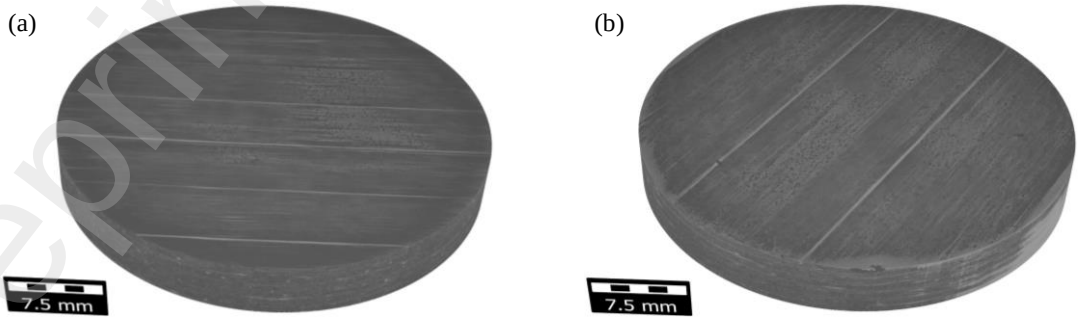

Figure 4. The reconstructed grey scale volumes of the preforms with (a) quarter-inch tape and (b) half-inch tape.

3. Virtual Permeability Prediction

3.1 Generation of Realistic Unit Cells

After scanning, the scanned images were reconstructed into 3D volumes and computational unit cells were created from these 3D volumes. From the raw volume of the circular specimens of each preform, a region of ineterest (ROI) was extracted. As the raw volumes were of digital nature, they can be oreinted in any directions and ROI's of different oreintations can be extracted. From each preform volume, two ROI's were extracted, one oreinted in the 0°/90° directions and the other orineted in ±45° orientations. The alignment of the edges of both types of unit cells were either in 0°/90° or ±45° directions. In this way, four in-plane permeability values (K_{+45}, K_{-45}, K_{00} and K_{90}) were computed. The channels and fiber tapes within the ROI were separated via global thresholding [34, 35]. The ROI's containing only the channels were treated as unit cells and used for digital flow experiments. The unit cells oriented in both 0°/90° and ±45° directions are shown in Figure 5. The unit cell sizes for the preforms with quarter and half inch tapes were 524×524×199 voxels (13.1×13.1×4.975 mm^3) and 1032×1032×198 voxels (25.8×25.8×4.95 mm^3), respectively. By design, the channels were expected to be 1.55% and 3.05% of the entire volume for the preforms with quarter and half inch tapes, respectively. The channel volume factions calculated from the unit cells (1.62% from 0°/90° unit cell and 1.49% from ±45° unit cell) of the preform with quarter inch tape were close to the design value (1.55%). However, the channel volume factions calculated from the unit cells (1.22% from 0°/90° unit cell and 1.34% from ±45° unit cell) of the preform with half inch tape were significantly less than the design value (3.05%). It can been seen in Figure 5 that some of the channels are discontinuous and some expected channels do not even exist. It could be partly because of the scanning resoultion which could not capture

the sub-micron channels. Also, the layup process may not have been able to keep the consistent channel size.

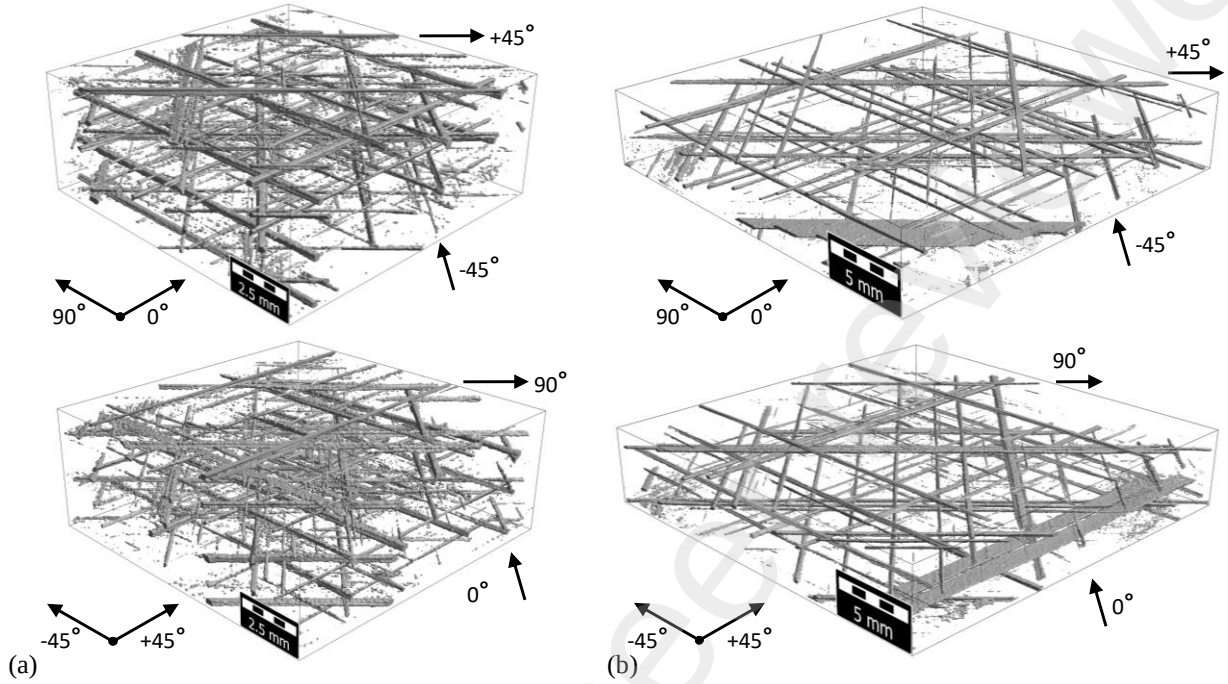

Figure 5. XCT based unit cell models oriented in 0°/90° and ±45°directions, (a) quarter-inch tape and (b) half-inch tape.

3.2 Statistical Analysis and Stochastic Modeling

Unit cells were also constructed using TexGen software with measurements taken from the scanned images. The XCT volume was sliced in 0°/90° and ±45°directions so that the cross-sections of the channels could be examined. A total number of 10 slices were extracted in each direction for both the preforms. The height and width of all the distinguishable channels were measured manually using MATLAB® [33]. The channel height and width measurements were statistically analyzed and it was observed that the variations in the height of the channels were statistically insignificant. Therefore, the height of the channels was assumed to be constant (0.2 mm) throughout the preform. However, a notable variation in the channel width measurements

was recorded, which was more pronounced in the half-inch tape. The variation in the channel width measurements (w) was modeled as a normal distribution given as,

$$f(w) = \frac{1}{\sigma\sqrt{2\pi}} e^{-\frac{1}{2}\left(\frac{w-\mu}{\sigma}\right)^2} \quad (3)$$

where, $f(w)$ is the frequency or probability of the width measurement, σ is the standard deviation and μ is taken as mean of the distribution. The frequency of the width measurements for both the performs along with their normal distributions are shown in Figure 6. As can be seen in Figure 6a, the channel width measurements for the quarter-inch tape possessed a single peak with a mean value of 0.15 mm. However, measurements for the half-inch tape showed two peaks having mean values of 0.17 mm and 1.11 mm. Hence, to generalize the probability distribution of the width measurement for both the preforms, a bimodal distribution has been adopted here. The generalized distribution model has two normal distributions along with one normal distribution and is given as,

$$f(w) = \rho_0 f_0(w) + \rho_1 f_1(w) + \rho_2 f_2(w) \quad (4)$$

ρ_0 is mixing parameter for channel width 0 mm, $f_0(w)$ is a uniform distribution and $f_1(w)$ and $f_2(w)$ are two normal distributions. The factors ρ_1 and ρ_2 are of the mixing parameters of the two normal distributions $f_1(w)$ (for channel width 0-0.5 mm) and $f_2(w)$ (for channel width > 1.0 mm), respectively. The normal distributions $f_1(w)$ and $f_2(w)$ are given by equation 1 and characterized by their mean values (μ) and standard deviations (σ). The values for each coefficient are given in Table 1.

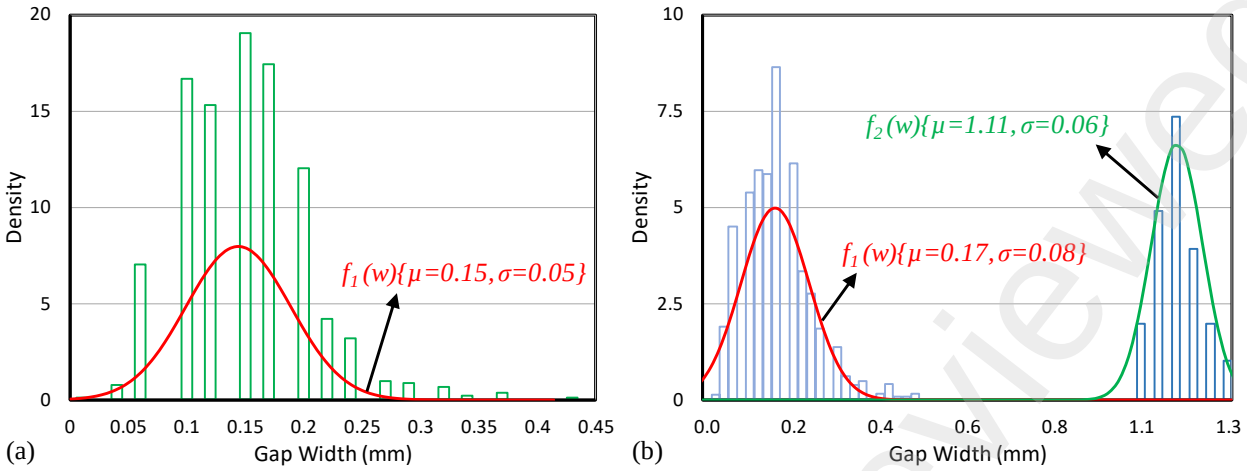

Figure 6. Probability distribution of channel width of the preforms with (a) quarter-inch tape and (b) half-inch tape.

Table 1. Generalized distribution model parameters measured from the channel width.

Parameter	Preform with Quarter inch tape	Preforms with Half-inch tape
ρ_0	0.33	0.20
$f_0(w)$	1	1
ρ_1	0.67	0.76
$f_1(w)$	σ = 0.05 and μ = 0.15	σ = 0.08 and μ = 0.17
ρ_2	0	0.04
$f_2(w)$	-	σ = 0.06 and μ = 1.11

3.2 Stochastic Unit Cells

The statistical models obtained here were used to create stochastic unit cell models in the TexGen software. The procedure for generating the models in TexGen software is outlined in Figure 7a. In the initial steps, the position, orientation and the height of the channels were defined. In the following steps, the channel width was defined ensuring its stochastic variation and the missing values were interpolated. The models were generated by extracting unit cells of desired size. An example of such a model generated in TexGen software is shown in Figure 7b. Finally, mesh files were created from the models and were run for the flow simulations. The orientation of the unit cells generated in TexGen were 0°/90° and are shown in Figure 8 for both the quarter and half inch

preforms. It is possible to generate unit cells in different orientations, however, they cannot be exported to another modeling framework. The models have a size of 400×400×192 voxels ($10\times10\times4.8mm^3$) with resolution of 25 µm. The percentage of the channel volumes in these models were 1.65% and 0.85% for the preforms with quarter and half inch tapes, respectively.

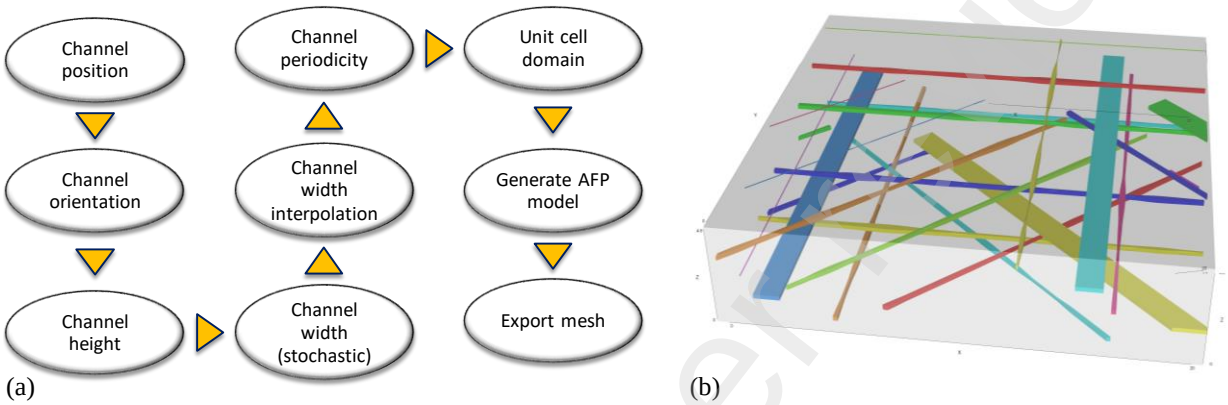

Figure 7. Strategy for stochastic modelling in TexGen, (a) steps and (b) an example model.

3.3 Digital Flow Simulations

The models generated direclty from the XCT images as well as the models generated stochastically in TexGen software were used in digitial flow simulations to compute the in-plane permeability. The numerical simulations were performed in GeoDict and ANSYS CFX. In GeoDict, the flow simulations were governed by Stokes equation while in ANSYS CFX, Navier-Stokes equations are responsible. In both cases, the simlations were setup in such a way to ensure very low Reynold's number and validity of Darcy's law. A pressure driven boundary condition with pressure differential applied across the faces normal to the direction of the flow was established, and the top and bottom faces were regarded as impermeable walls. This was achieved in the simulation package by using periodic boundary conditions. The interface between the channels and carbon fiber tapes were assumed as impermeable wall. The in-plane permeability predictions

were solely based on flow within the channels and ignoring the microscale permeability through the tapes which was found to be very negligible [24]. In GeoDict, the unit cells were extracted in such a way that the faces were aligned to the coordinate system. However, in ANSYS CFX, the unit cell had to be rotated as shown in Figure 9. Because of better compatibility of TexGen with ANSYS CFX and a numnber of unit cells were used.

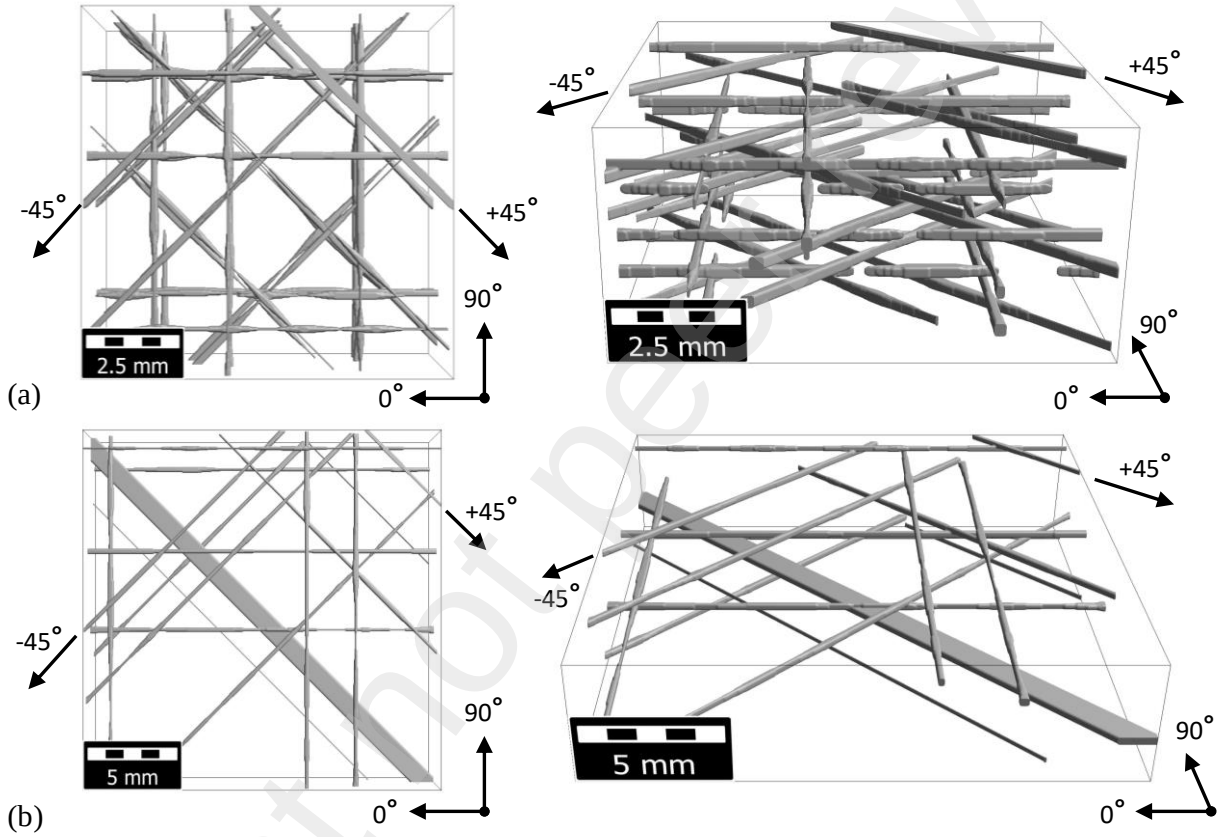

Figure 8. Top view and 3D view of the 0°/90° oriented TexGen stochastic models of the preforms with (a) quarter inch tape and (b) half inch tape.

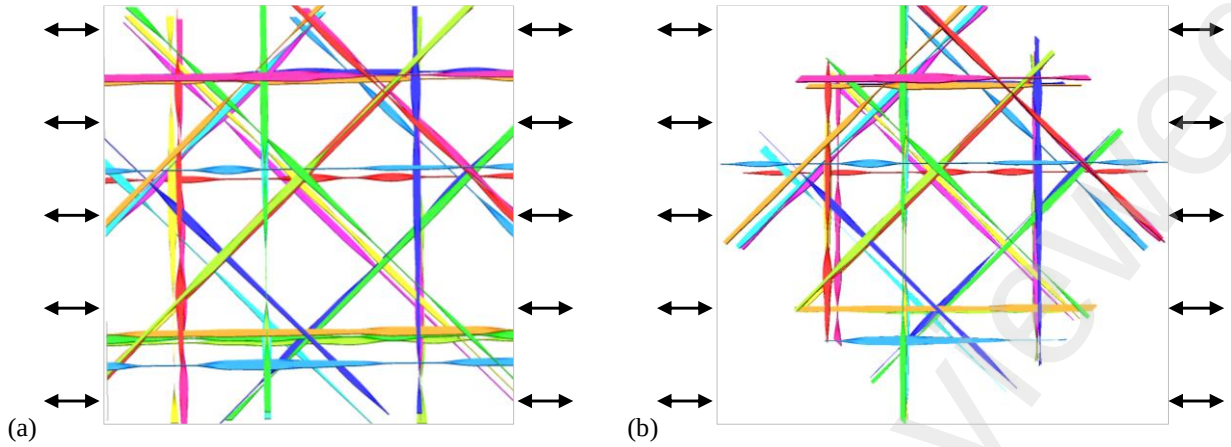

Figure 9. Boundary conditions used in ANSYS CFX, (a) normal and (b) rotated.

4. Results and Discussion

4.1 In-plane permeability measurement

The flow front progression at various time steps is shown in Figure 10 for both types of preforms. The flow front seems to be irregular in shape and flowing predominantly through the channels. The minor and major axes of the fitted ellipse were found to be aligned with the channels. The flow front tracking yields transient in-plane permeability using equations (1) and (2). Although it was expected that the in-plane permeability of quarter-inch tape preforms would be higher, but due to variability in the layup process, the channels were larger than the target channel of 0.2 mm in the half-inch tape preforms [24]. Figure 8 shows fluctuation of permeability at the start of the experiment, and constant behavior once a steady state flow was established, this trend being more obvious in the half-inch tape preforms due to greater amount of variability in the channels. The final values are given in Table 2 in section 4.3 and compared with the virtually predicted values. Note, that these values are based on the flow front positions at the bottom of the test sample. The transient flow permeability may not be ideal for AFP preforms, as the captured flow front profiles show the flow only through the layer oriented in +45° direction and the flow pattern in the interior layers may be considerably different. Saturated permeability measurement techniques (similar to

through thickness permeability measurements) may result in better representation of permeability values in these types of preforms.

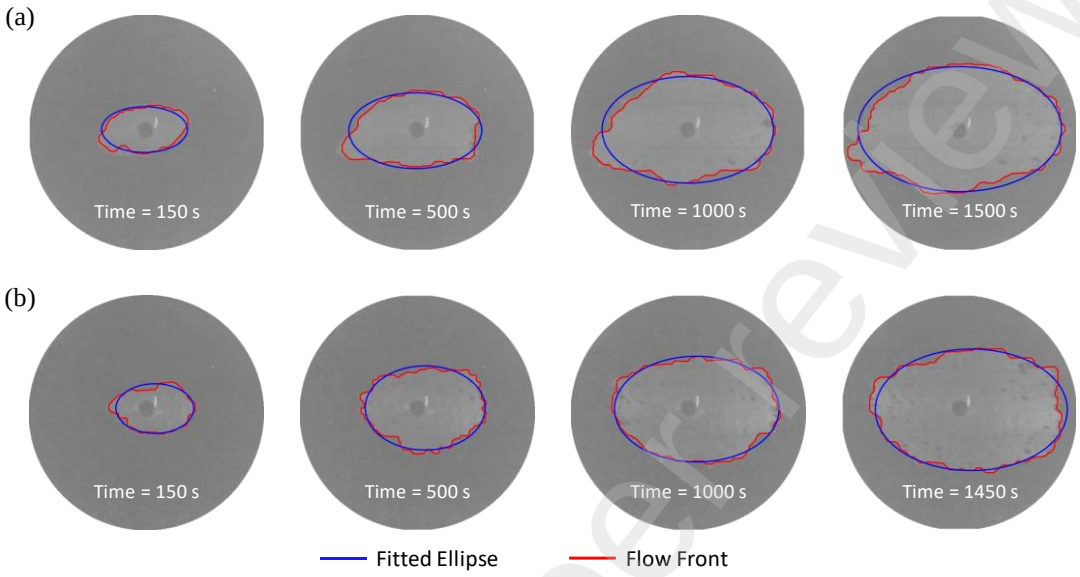

Figure 10. Flow front progression in the preforms with (a) quarter-inch tape and (b) half-inch tape preforms.

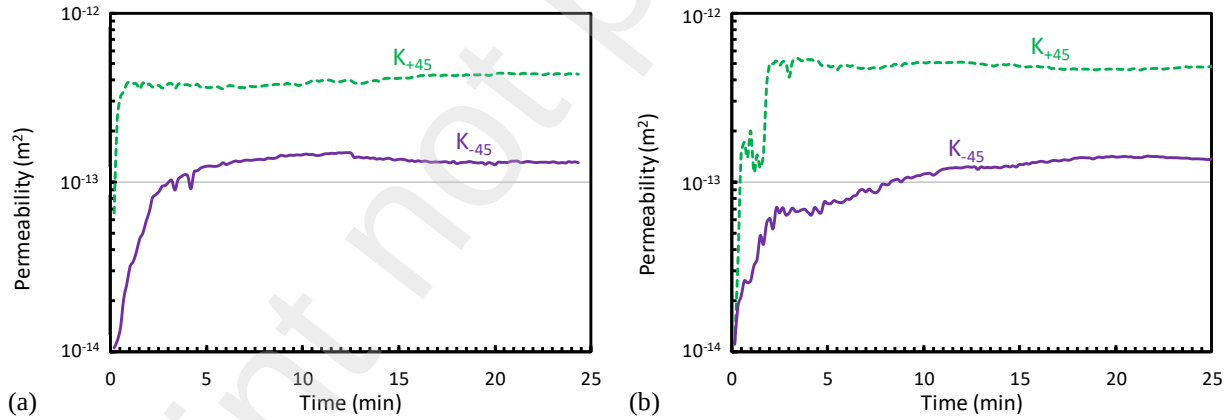

Figure 11. Transient permeability measurements of the preforms with (a) quarter-inch tape and (b) half-inch tape.

4.2 Flow patterns through the channels

The digital flow simulation provides detailed idea about the flow pattern through the channels. The flow field velocity obtained from GeoDict simulations on XCT models in various direction for the two preforms are given in Figures 12 and 13. Similarly, the flow pattern from GeoDict simulations

on TexGen models in 0/90 direction for the two preforms are given in Figure 14. All the figures suggest that all of the channels were responsible for fluid flow. However, the channels aligned with the flow contributes more. In all the simulations, the maximum flow velocity is in the order of 10^{-5} m/s. However, the overall number of channels contributing to the flow in the TexGen models is lower than that in the µCT models. As a result, the permeability values computed from the µCT models were relatively higher than the values computed from the TexGen models, as presented in Table 2 in the next section. In the TexGen model of half-inch tape, Figure 14 (b), there is one relatively large channel, oriented in the -45° direction, that has openings on both the 0° and 90° faces. Hence, this channel contributes to the flow in both cases whether the pressure gradient is across the 0° faces and or the 90° faces.

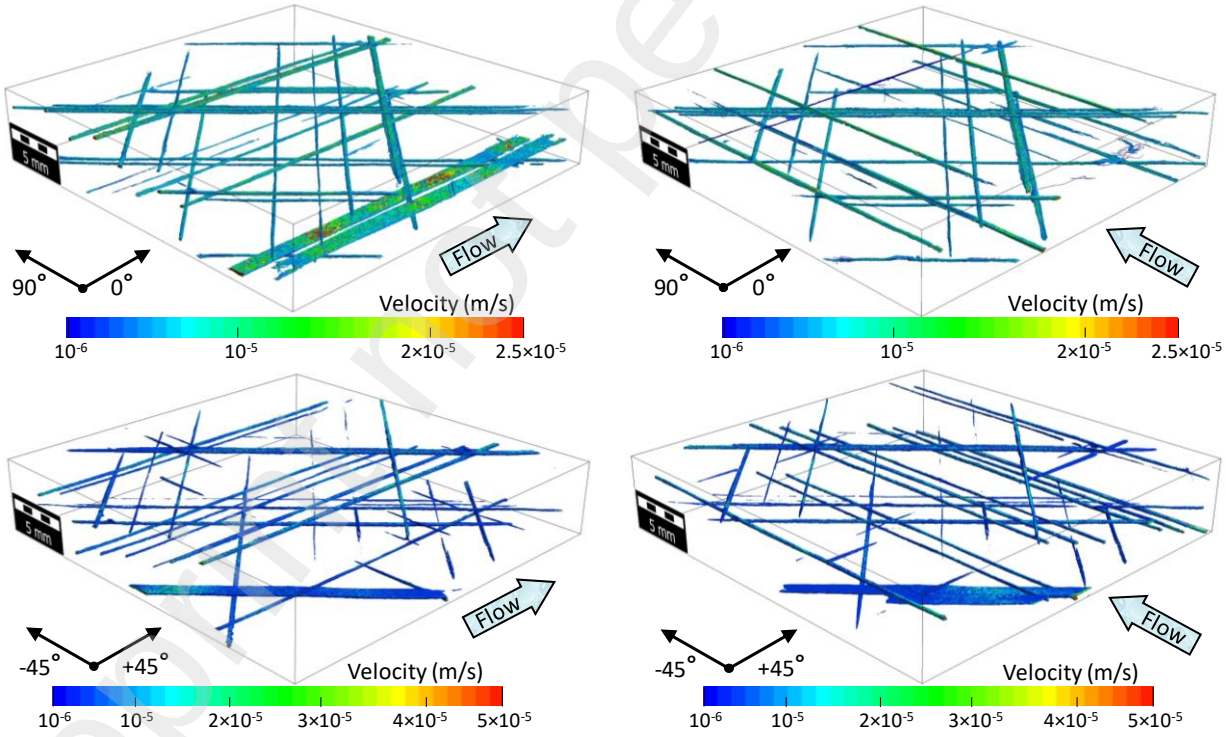

Figure 12. Visualization of the velocity field obtained from the µCT-GeoDict models in 0°/+45°/90°/-45° directions of the preform with quarter-inch tape.

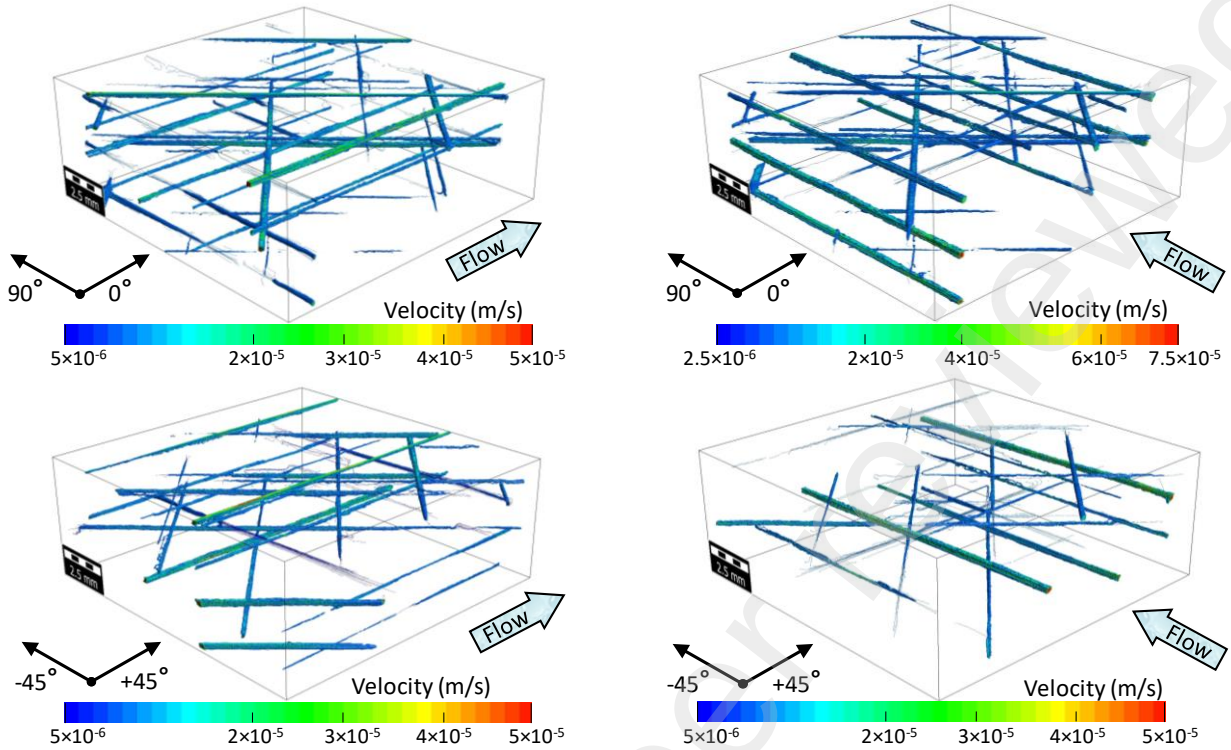

Figure 13: Visualization of the velocity field obtained from the μCT-GeoDict models in 0°/+45°/90°/-45° directions of the preform with half-inch tape.

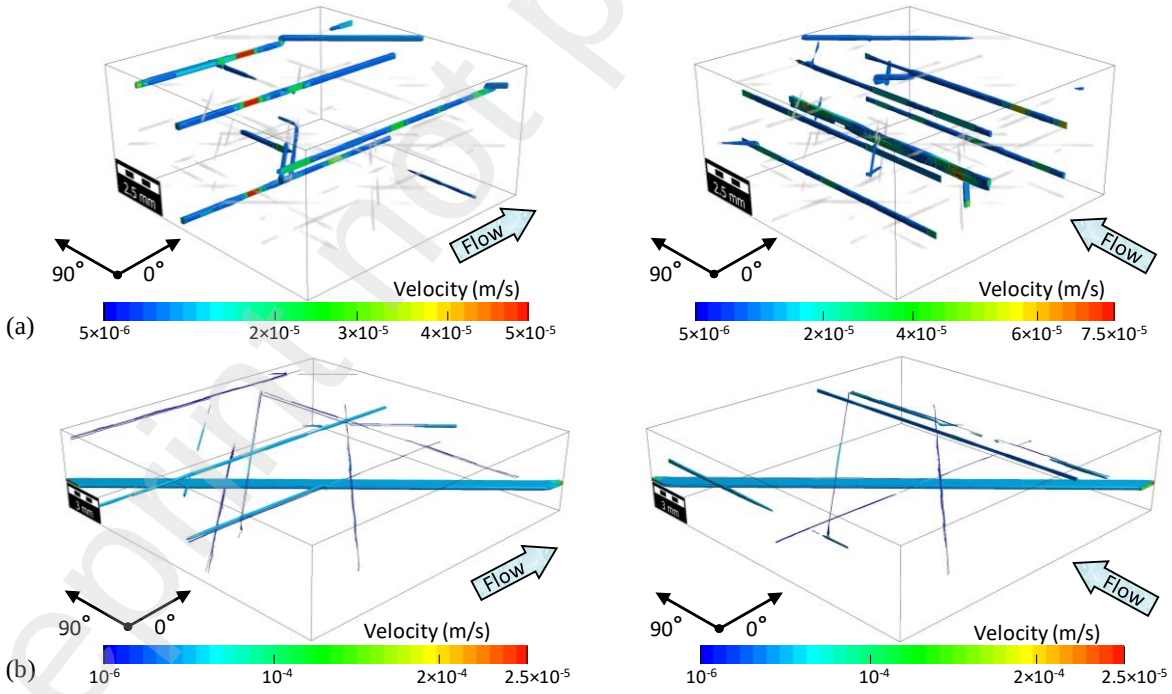

Figure 14. Visualization of the velocity field obtained from the TexGen-GeoDict models of the preforms with (a) quarter-inch tape and (b) half-inch tape.

4.3 Virtual Permeability Predictions

The predicted permeability values were compared with experimentally measured values and presented in Table 2. In Table 2, the values presented are from the experimental measurements and three different modeling approaches. As mentioned before, in-plane permeability were measured from experiments was along ±45° orientations. It was possible to generate unit cells in any desired orientation from µCT images. Hence, the GeoDict simulations using unit cells generated from µCT images yielded in-plane permeability values along the ±45° orientations as well as 0/90° orientations, as listed in Table 2. Due to compatibility issues, the stochastic unit cells generated using TexGen used for flow simulations in GeoDict were oriented in 0/90° orientations only. As an alternative, ANSYS-CFX was selected for flow simulations using the stochastic unit cells. The values obtained from virtual in-plane permeability of carbon fiber AFP tapes were computed using both stochastic and realistic approaches. Additional models (stochastic) were also generated to assess the variability of the predictions. All the predictions by µCT-GeoDict were in the order of 10^{-12} m^2 albeit significantly deviated from the experimentally measured values. Since, the experimentally measured values were based on the flow front positions in the layer oriented in +45° direction only, the deviations were anticipated. The permeability values obtained from TexGen models showed similar trends as the computed ones. However, the permeability values computed from the µCT models were relatively higher than the values computed from the TexGen models, due to higher number of effective channels in the µCT models. Only, the TexGen model of the half-inch tape predicted higher values than their µCT counterpart. This is because of the relatively large channel in the TexGen model, as discussed in the previous section. Based on the significant variation in these values, it can be concluded that the AFP presents a major challenge to obtain consistent permeability values regardless of the modeling approach employed.

Table 2. Permeability values of the preforms in different orientations.

Preform	Orientation	Permeability ($\times 10^{-12}$ m^2)			
		Experiment	μCT-GeoDict	TexGen-GeoDict	TexGen-CFX
Half inch tape	+45°	1.42	2.44	--	2.28
	0°	--	3.51	9.58	4.21
	-45°	0.183	6.58	--	1.46
	90°	--	4.29	9.65	2.57
Quarter inch tape	+45°	0.541	1.52	--	0.612
	0°	--	2.20	0.557	0.666
	-45°	0.284	1.07	--	0.770
	90°	--	2.04	0.980	0.828

As mentioned in the previous section, there is a difference of up to one order of magnitude between the experimentally measured and numerically predicted permeability values, demonstrating the complexity of AFP laid preforms. In the cases studied here, the variability in the channels was very high; hence the inconsistency in the permeability was also notably high. The variability in the predictions were further investigated using 7 stochastic models generated in TexGen. The flow simulations using these stochastic models were performed in ANSYS CFX. The permeability values predicted from these stochastic models are presented in Figure 15. In Figure 15, the columns represent the individual values whereas the dashed line represent the mean values. The computed values were not even within the same orders of magnitude rather spread substantially. The coefficients of variance for these values were in the range of 75-130%. These variations in the computed values reinforces the notion that the AFP presents a major challenge to obtain consistent permeability values.

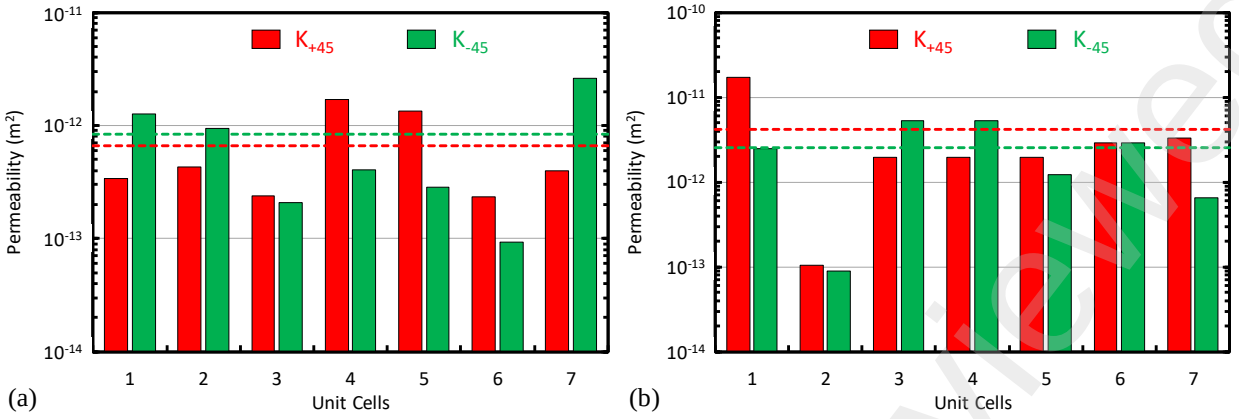

Figure 15. The variation in the virtual permeability predictions among various unit cells of the preforms with (a) quarter and (b) half inch carbon tapes.

5. Conclusions

In this work, we have highlighted the challenges in achieving spatial uniformity in the automated fiber placement approach and investigated the correlation between the spatial variability of the preforms and the in-plane permeability. Realistic geometric models for numerical permeability predictions were obtained using XCT based characterization framework. The framework was utilized to scan two types of preforms with different tape width based on which realistic and stochastic geometric models were generated. The in-plane permeability values were computed numerically using these models. A standard benchmark permeability measurement set-up was utilized to obtain transient experimental in-plane preform permeability through 2D radial mold filling. The numerical permeability values were compared with experimental values.

The XCT based statistical analysis showed that the variations in channel height was insignificant. However, a notable variation in the channel width measurements was recorded, which was more pronounced in the half-inch tape preforms. The flow fields suggest that all the channels participated in the transport of the fluid. However, the channels aligned with the flow direction contribute more. All the numerical predictions deviated from the experimentally measured values

by approximately one order of magnitude. Moreover, the numerically predicted values using the stochastic models also showed scatter with a coefficient of variance of 75-130%. Based on the variations in these values, it can be concluded that AFP process presents a major challenge to layup tapes with consistent widths, which may result in inconsistent experimental and numerical permeability values throughout the preform. However, the XCT based stochastic modeling technique is an effective and attractive way to estimate the permeability of dry fiber preforms virtually.

6. Acknowledgements

The authors acknowledge the funding received from Khalifa University of Science and Technology, internal research fund CIRA-2020-007 grant number 8474000275. The authors would also like to thank Dr. Xuesen Zeng from the University of Southern Queensland, Australia for helping in stochastic modeling and Dr. RA Alia for helping in the permeability measurements.

Data availability statement:

The raw/processed data required to reproduce these findings cannot be shared at this time as the data also forms part of an ongoing study.

References:

[1] A. Endruweit, X. Zeng, A. Long, Multiscale modeling of combined deterministic and stochastic fabric non-uniformity for realistic resin injection simulation, Advanced Manufacturing: Polymer & Composites Science 1(1) (2015) 3-15.
[2] N. Kuentzer, P. Simacek, S.G. Advani, S. Walsh, Permeability characterization of dual scale fibrous porous media, Composites Part A: Applied Science and Manufacturing 37(11) (2006) 2057-2068.
[3] M. Yun, T. Carella, P. Simacek, S. Advani, Stochastic modeling of through the thickness permeability variation in a fabric and its effect on void formation during Vacuum Assisted Resin Transfer Molding, Composites Science and Technology 149 (2017) 100-107.
[4] H.S. Sas, E.B. Wurtzel, P. Simacek, S.G. Advani, Effect of relative ply orientation on the through-thickness permeability of unidirectional fabrics, Composites Science and Technology 96 (2014) 116-121.

[5] J.H. Z., U. Rehan, C.W. J., Skin-core debonding in resin-infused sandwich structures, Polymer Composites 37(10) (2016) 2974-2981.
[6] K. Croft, L. Lessard, D. Pasini, M. Hojjati, J. Chen, A. Yousefpour, Experimental study of the effect of automated fiber placement induced defects on performance of composite laminates, Composites Part A: Applied Science and Manufacturing 42(5) (2011) 484-491.
[7] D.H.J.A. Lukaszewicz, C. Ward, K.D. Potter, The engineering aspects of automated prepreg layup: History, present and future, Composites Part B: Engineering 43(3) (2012) 997-1009.
[8] R. Umer, S. Rao, J. Zhou, Z. Guan, W.J. Cantwell, The low velocity impact response of nano modified composites manufactured using automated dry fibre placement, Polymers and Polymer Composites 24(4) (2016) 233-240.
[9] H. Parmar, T. Khan, F. Tucci, R. Umer, P. Carlone, Advanced robotics and additive manufacturing of composites: towards a new era in Industry 4.0, Materials and Manufacturing Processes 37(5) (2022) 483-517.
[10] D. Becker, P. Mitschang, Influence of preforming technology on the out-of-plane impregnation behavior of textiles, Composites Part A: Applied Science and Manufacturing 77 (2015) 248-256.
[11] O. Rimmel, D. Becker, P. Mitschang, Maximizing the out-of-plane-permeability of preforms manufactured by dry fiber placement, Advanced Manufacturing: Polymer & Composites Science 2(3-4) (2016) 93-102.
[12] J. Sloan, ATL and AFP: Defining the megatrends in composite aerostructures, CompositesWorld, 2008.
[13] K. Kozaczuk, Automated fiber placement systems overview, Prace Instytutu Lotnictwa (4 (245)) (2016) 52-59.
[14] N. Hassan, J.E. Thompson, R.C. Batra, A.B. Hulcher, X. Song, A.C. Loos, A heat transfer analysis of the fiber placement composite manufacturing process, Journal of Reinforced Plastics and Composites 24(8) (2005) 869-888.
[15] P.A. Kelly, R. Umer, S. Bickerton, Viscoelastic response of dry and wet fibrous materials during infusion processes, Composites Part A: Applied Science and Manufacturing 37(6) (2006) 868-873.
[16] K.A. Khan, R. Umer, Modeling the viscoelastic compaction response of 3D woven fabrics for liquid composite molding processes, Journal of Reinforced Plastics and Composites 36(18) (2017) 1299-1315.
[17] C.D. Rudd, M.R. Turner, A.C. Long, V. Middleton, Tow placement studies for liquid composite moulding, Composites Part A: Applied Science and Manufacturing 30(9) (1999) 1105-1121.
[18] M. Assadi, T. Field, AFP processing of dry fiber carbon materials (DFP) for improved rates and reliability, SAE International Journal of Advances and Current Practices in Mobility 2(3) (2020) 1196-1201.
[19] X. Xiao, A. Endruweit, X. Zeng, J. Hu, A. Long, Through-thickness permeability study of orthogonal and angle-interlock woven fabrics, Journal of Materials Science 50(3) (2015) 1257-1266.
[20] H. Alhussein, R. Umer, S. Rao, E. Swery, S. Bickerton, W.J. Cantwell, Characterization of 3D woven reinforcements for liquid composite molding processes, Journal of Materials Science 51(6) (2016) 3277-3288.
[21] P. Bhat, J. Merotte, P. Simacek, S.G. Advani, Process analysis of compression resin transfer molding, Composites Part A: Applied science and manufacturing 40(4) (2009) 431-441.

[22] O. Rimmel, D. May, P. Mitschang, Impact of stitching on permeability and mechanical properties of preforms manufactured by dry fiber placement, Polymer Composites 40(4) (2019) 1631-1642.
[23] G. Rieber, P. Mitschang, 2D Permeability changes due to stitching seams, Composites Part A: Applied Science and Manufacturing 41(1) (2010) 2-7.
[24] A. Aziz, M. Ali, X. Zeng, R. Umer, P. Schubel, W. Cantwell, Transverse permeability of dry fiber preforms manufactured by automated fiber placement, Composites Science and Technology 152 (2017) 57-67.
[25] P.B. Nedanov, S.G. Advani, Numerical computation of the fiber preform permeability tensor by the homogenization method, Polymer composites 23(5) (2002) 758-770.
[26] M. Belhaj, M. Deleglise, S. Comas-Cardona, H. Demouveau, C. Binetruy, C. Duval, P. Figueiredo, Dry fiber automated placement of carbon fibrous preforms, Composites Part B: Engineering 50 (2013) 107-111.
[27] M. Bodaghi, A. Vanaerschot, S.V. Lomov, N. Correia, On the variability of mesoscale permeability of a 2/2 twill carbon fabric induced by variability of the internal geometry, Composites Part A: Applied Science and Manufacturing 101 (2017) 394-407.
[28] X. Zeng, A. Endruweit, L.P. Brown, A.C. Long, Numerical prediction of in-plane permeability for multilayer woven fabrics with manufacture-induced deformation, Composites Part A: Applied Science and Manufacturing 77 (2015) 266-274.
[29] J.R. Weitzenböck, R.A. Shenoi, P.A. Wilson, Radial flow permeability measurement. Part A: Theory, Composites Part A: Applied Science and Manufacturing 30(6) (1999) 781-796.
[30] J.R. Weitzenböck, R.A. Shenoi, P.A. Wilson, Radial flow permeability measurement. Part B: Application, Composites Part A: Applied Science and Manufacturing 30(6) (1999) 797-813.
[31] D. May, A. Aktas, S.G. Advani, D.C. Berg, A. Endruweit, et al., In-plane permeability characterization of engineering textiles based on radial flow experiments: A benchmark exercise, Composites Part A: Applied Science and Manufacturing 121 (2019) 100-114.
[32] M.A. Ali, R. Umer, K.A. Khan, S. Bickerton, W.J. Cantwell, Non-destructive evaluation of through-thickness permeability in 3D woven fabrics for composite fan blade applications, Aerospace Science and Technology 82-83 (2018) 520-533.
[33] M.A. Ali, R. Umer, K.A. Khan, Experimental-Numerical Hybrid Reinforcement Characterization Framework, CT Scan Generated Material Twins for Composites Manufacturing in Industry 4.0, Springer Singapore, Singapore, 2020, pp. 73-94.
[34] M.A. Ali, R. Umer, K.A. Khan, A virtual permeability measurement framework for fiber reinforcements using micro CT generated digital twins, International Journal of Lightweight Materials and Manufacture 3(3) (2020) 204-216.
[35] M.A. Ali, R. Umer, K.A. Khan, W.J. Cantwell, Application of X-ray computed tomography for the virtual permeability prediction of fiber reinforcements for liquid composite molding processes: A review, Composites Science and Technology 184 (2019) 107828.